



Efficient and Spatially Controlled Functionalization of SBA-15 and Initial Results in Asymmetric Rh-Catalyzed 1,2-Additions under Confinement

Ann-Katrin Beurer,^[a] Manuel Kirchhof,^[b] Johanna R. Bruckner,^[c] Wolfgang Frey,^[b] Angelika Baro,^[b] Michael Dyballa,^[a] Frank Giesselmann,^[c] Sabine Laschat,^[b] and Yvonne Traa*^[a]

Selectively functionalized mesoporous silica may considerably advance heterogeneous catalysis through the controlled immobilization of highly selective complex catalysts inside the mesopores. However, spatially controlled functionalization and the precise analytical verification are still a challenge. In this publication, we report a method, which ensures a selective functionalization of the mesopore surface with a clickable linker and thus makes it possible to study confinement effects during catalyzed reactions. First, we passivate the silanol groups on the

particle surface and in the pore entrances of the mesoporous silica material SBA-15 with 1,1,1-trimethyl-*N*-(trimethylsilyl) silanamine. Then we remove the template by solvent extraction and functionalize the pore walls with 3-azidopropyltriethoxysilane before we click the catalyst. In initial experiments of asymmetric Rh-catalyzed 1,2-addition, we investigate the performance of a catalyst clicked selectively in the mesopores and compare it to the dissolved catalyst as well as to the catalyst immobilized exclusively on the external surface of SBA-15.

Introduction


Since their discovery in 1992,^[1] ordered mesoporous silica materials (MSMs) have received substantial scientific interest and set the benchmark for all mesoporous materials. In general, the production of most inorganic mesoporous materials is based on the use of organic template molecules. They are brought into solution before the inorganic precursor molecules are added. The precursor molecules deposit around the micelle-like structure of the template and condense into a mesoporous material whose pores are filled with the template.^[2] After the mesoporous material is produced, the pores are closed and must be opened after the synthesis.^[3] MSMs can easily be synthesized with adjustable pore diameter, a narrow pore size


distribution, surfaces of more than 700 m²g⁻¹ and a high thermal stability. As a result, they became indispensable in present applications. MSMs are mainly used in heterogeneous catalysis,^[4] in separation processes,^[5] as sensors,^[5] or in biomedicine, for example, as drug delivery system.^[6] A method to even increase the application range of MSMs is to modify their surface, e.g., by grafting, immobilization and ion exchange.^[7,8] During grafting, the functional groups of the reagent are bound to the surface silanol groups by a condensation reaction after the synthesis of the MSMs. However, it cannot be controlled if the functionalization takes place on the particle surface or the internal surface.^[7] Therefore, it must be taken into account that MSMs have two different surfaces. Firstly, there is the particle surface, which is typically smaller, but easily accessible. Secondly, there is the internal surface, which represents the larger proportion, but is more difficult to access.^[7] Regarding the application of silica, it is often necessary to functionalize the different surfaces selectively in order to determine the location of the modification and to use confinement effects. For the selective functionalization of the particle surface and the internal surface of the MSMs, two methods are feasible – the diffusion-controlled method and the pore protection process.^[7] During the diffusion-controlled method, the particle surface of calcined or extracted MSMs is functionalized in the first step. Afterwards, the pore walls are modified. The diffusion-controlled method is only suitable for porous materials with small pores (2–3 nm). The reason for this is that very large, bulky organosilanes, which are not able to enter the pores, must be employed to functionalize the particle surface.^[5,9,10] By contrast, the pore protection process is suitable for functionalizing porous materials for all pore diameters.^[9,11] The pore protection process uses either as-synthesized silica, the pores of which are blocked by


[a] A.-K. Beurer, Dr. M. Dyballa, Apl. Prof. Y. Traa
Institute of Technical Chemistry
University of Stuttgart
70569 Stuttgart (Germany)
E-mail: yvonne.traa@itc.uni-stuttgart.de

[b] M. Kirchhof, Dr. W. Frey, Dr. A. Baro, Prof. S. Laschat
Institute of Organic Chemistry
University of Stuttgart
70569 Stuttgart (Germany)

[c] Dr. J. R. Bruckner, Prof. F. Giesselmann
Institute of Physical Chemistry
University of Stuttgart
70569 Stuttgart (Germany)

 Supporting information for this article is available on the WWW under <https://doi.org/10.1002/cctc.202100229>

 This publication is part of a Special Collection on "Catalysis in Confined Spaces". Please check the ChemCatChem homepage for more articles in the collection.

 © 2021 The Authors. ChemCatChem published by Wiley-VCH GmbH. This is an open access article under the terms of the Creative Commons Attribution License, which permits use, distribution and reproduction in any medium, provided the original work is properly cited.

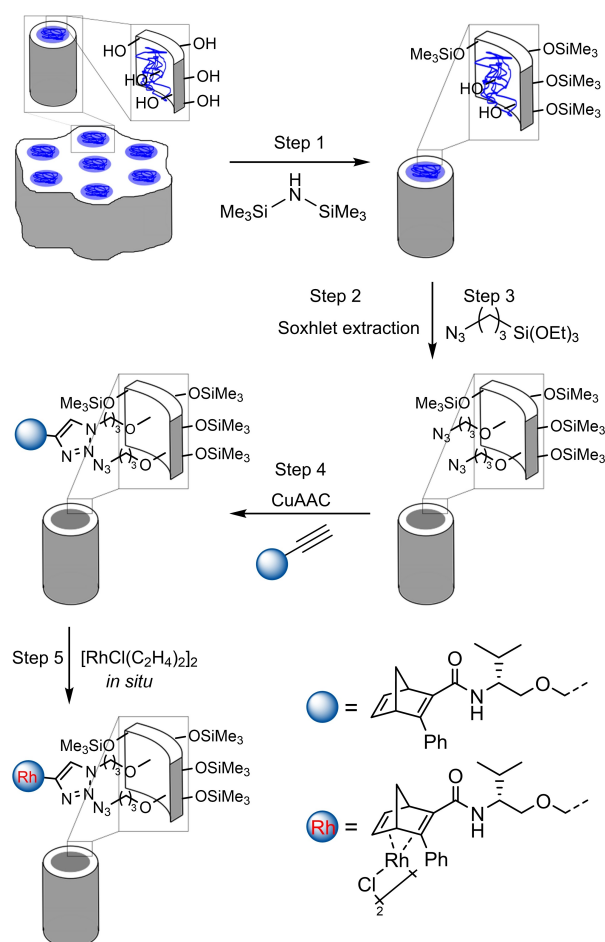
template used during the synthesis,^[7,12] or calcined silica, whose pores are refilled with template or another polymer (e.g., methyl methacrylates).^[13] Thus, only the silanol groups of the particle surface are accessible for the functionalization reagent. It should be noted that the modification does not only functionalize the particle surface of the as-synthesized silica, but also parts of the pore walls. This is due to the fact that a small proportion of pores in the as-synthesized SBA-15 is not blocked with template. As a result, the functionalizing reagent can also penetrate into these pores and functionalize the silanol groups there.^[11] Furthermore, previous work shows that organosilanes with chloro or ethoxy groups extract template from the pore entrances due to the amphiphilic character of the triblock copolymer P123, which is used as template.^[7,13–16] Nevertheless, chloro-, methoxy- or ethoxysilanes are often used to functionalize the particle surface.^[13] After functionalizing the particle surface and removing the template from the pores by extraction or calcination, the internal surface can be modified.^[7,12]

The functionalization of the porous materials is of great importance to obtain catalysts for further applications. Many different reactions have been described, which are performed on metal-supported silica. For example, Dixit et al. investigated the dehydrogenation of benzyl alcohol on silica-supported copper catalysts.^[17] Another field of application is the catalytic reduction of NO on copper oxide supported on silica done by Patel et al.^[18] In addition, the literature is very much concerned with cross-coupling reactions performed on palladium-supported silica.^[19] Furthermore, oxidation reactions were performed on supported silica, e.g., the selective oxidation of alcohols^[20] or sulfides^[21] on mesoporous silica with grafted oxovanadium Schiff bases.

The efficient and spatially controlled functionalization of porous materials could also be of great importance for the formation of stereoselective products similar to the functionality of enzymes. The porous properties of the support should help to form the desired configuration of the product. In order to take advantage of the porous structure of the support for the formation of stereoselective products, it is important to ensure that the catalytically active sites are located exclusively in the mesopores after the inertization of the particle surface of the support. However, a proven method to achieve this goal is not available yet. In the literature, several approaches for the selective functionalization of silica have been reported. For example, Yang et al. functionalized the micropores of mesoporous SBA-15 with Pd and assumed that all accessible silanol groups on the particle surface and the mesoporous walls are not able to bind the metal.^[22] Liu et al. functionalized MCM-41 via a stepwise procedure by treatment of the external surface with mercaptopropyltrimethoxysilane, extraction of the template with an acidic ethanol solution and functionalization of the pore walls with 3-azidopropyltriethoxysilane.^[23] Webb et al. described the stepwise functionalization of SBA-15 and refilled the pores before the functionalization procedure to be sure that only the particle surface is functionalized and not the pore entrances as well. After the refill step, they functionalized the particle surface with hexamethyl disilazane, removed the

template with Soxhlet extraction and modified the pore walls with mercaptopropyltrimethoxysilane.^[24] However, these reports did not unequivocally demonstrate that selective functionalization of the inner pore walls was achieved while the particle surface was left inert. In order to obtain unambiguously only the functionalization of the inner mesopore walls, we implemented a control step (see Results and Discussion). In addition, by combining several characterization techniques, we could prove that the final catalyst was immobilized exclusively on the mesopore walls.

In greater detail, the selective functionalization of SBA-15 proposed in this work is based on the pore protection process (Scheme 1). The functionalization of the particle surface of as-synthesized SBA-15 is carried out with 1,1,1-trimethyl-*N*-(trimethylsilyl)silanamine (HMDS) as a functionalization reagent (Scheme 1, Step 1). The inertization of the external surface is checked by a separate, independent control step (see Results and Discussion). Afterwards, the structure-directing template is removed by Soxhlet extraction after the complete functionalization of the particle surface (Scheme 1, Step 2). The pore walls of the mesopores are then functionalized with 3-azidopropyltriethoxysilane (AzPTES) (Scheme 1, Step 3). Subsequent click anchor-



Scheme 1. Procedure for the controlled and selective functionalization of mesoporous materials, followed by immobilization of the diene ligand and final in situ Rh complexation to obtain the immobilized Rh catalyst.

ing of the alkynyl-functionalized diene ligand via Cu-catalyzed azide-alkyne cycloaddition (CuAAC) (Scheme 1, Step 4) gives the immobilized ligand, followed by *in situ* complexation with the Rh precursor complex $[\text{RhCl}(\text{C}_2\text{H}_4)_2]_2$ to give the immobilized Rh catalyst (Scheme 1, Step 5). CuAAC has been successfully employed for the immobilization of various complex catalysts.^[21,25,26] However, there are no examples for the immobilization of Rh diene complexes on silica through CuAAC in the literature. Finally, in order to probe confinement effects of the functionalized SBA-15 on the enantioselective catalysis, the asymmetric 1,2-addition of triphenylboroxine to *N*-tosylimines catalyzed by chiral Rh diene complexes was chosen as a model reaction. The corresponding homogeneously Rh-catalyzed 1,2-addition has been extensively studied and various diene ligands have been developed.^[27–29] However, until now the influence of a solid confinement provided by tailored mesoporous silica on the catalytic activity and enantioselectivity of Rh diene complexes has not been investigated. Thus, the aim of the present study was to show that the chiral Rh-containing complexes are located *exclusively* in the mesopores of SBA-15 and can effectively control the enantioselectivity in the 1,2-addition of triphenylboroxine to *N*-tosylimines.

Results and Discussion

Synthesis of SBA-15

The starting material for the efficient and spatially controlled functionalization was as-synthesized SBA-15. The as-synthesized SBA-15 shows the characteristic reflexes d_{100} , d_{110} and d_{200} (Figure S21) which confirm the hexagonal structure (*p6mm*) of SBA-15.^[2] The N_2 physisorption measurement of the calcined SBA-15 shows the isotherm typical for SBA-15 (Figure S1) from which the surface area and pore volume as well as the pore diameter were determined and which are listed in Table 1 and Table S1. The results correspond to the characteristic values found in literature.^[2]

Explanation of the nomenclature

For a better understanding of the present work, the nomenclature of the different samples is introduced at this point. In Scheme 2, the sample designations are assigned to the corresponding materials. If SBA-15 is mentioned directly after the synthesis, it is called *as-synthesized SBA-15*. The pores of the as-synthesized SBA-15 are sealed with the triblock copolymer P123 and silanol groups are located on the particle surface. As a reference material, SBA-15 with opened pores is used in this paper. It is called *calcined SBA-15* and its pores were opened by the calcination step. To obtain the selectively functionalized catalyst, the external surface of the as-synthesized SBA-15 is functionalized in a first step. The material with functionalized particle surface is named *SBA-15-ex*. In the next step, the triblock copolymer P123 used as a template is removed from the pores of the as-synthesized SBA-15 by Soxhlet extraction

Table 1. Total surface determined by the BET method (S_{BET}), external surface (S_{external}) and micropore surface (S_{micro}) of as-synthesized, calcined and selectively functionalized SBA-15. Furthermore, the pore diameter determined by the DFT method ($d_{\text{pore,DFT}}$) and the lattice parameter a determined from the X-ray measurements are listed. The azide concentration c_{N_3} was determined by elemental analysis.

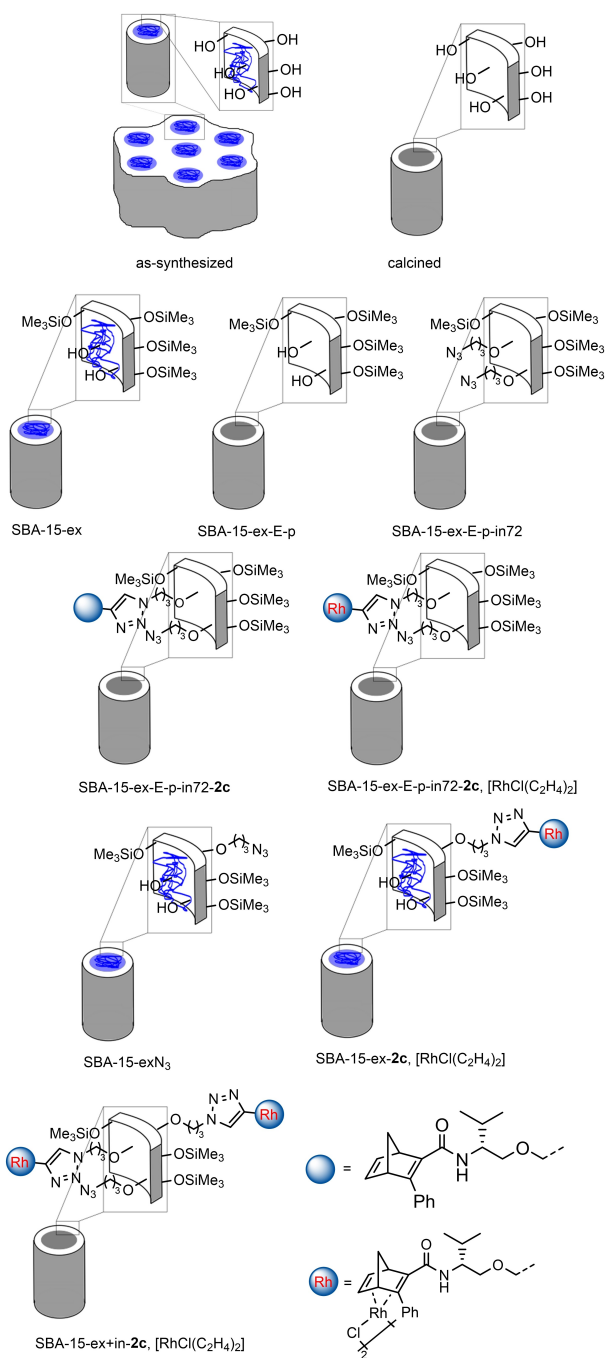
SBA-15 ^[a]	S_{BET} [m^2g^{-1}]	$S_{\text{external}}^{\text{[b]}}$ [m^2g^{-1}]	S_{micro} [m^2g^{-1}]	$d_{\text{pore,DFT}}$ [nm]	a [nm]	c_{N_3} [mmol g^{-1}]
as-synthesized	80	80	0	7.03	12.4	–
calcined	926	614	311	7.03	11.4	–
-ex	281	281	0	7.56	12.6	–
-ex-control	504	504	0	7.59	12.6	–
-ex-E	518	518	0	7.59	12.6	–
-ex-E-p	788	509	279	7.31	11.7	–
-ex-E-in6	611	611	0	7.56	12.6	–
-ex-E-p-in6	625	472	152	7.31	11.7	$3.41 \cdot 10^{-2}$
-ex-E-p-in24	826	614	212	7.31	11.7	$8.96 \cdot 10^{-2}$
-ex-E-p-in72	723	562	162	7.31	11.7	$1.23 \cdot 10^{-1}$

[a] The sample names include the following abbreviations: -ex denotes HMDS functionalization on the external particle surface; -control denotes the control step with AzPTES; -E denotes extraction with EtOH; -p denotes pretreatment in N_2 ; in6, in24 and in72 denote the functionalization time of the internal mesopores with AzPTES. [b] The so-called external surface determined from the N_2 physisorption measurements consists of the particle surface and of the surface of all pores larger than micropores.

(abbreviated with an “E”). In a pretreatment step, the silanol groups on the pore walls are converted into freely accessible silanol groups (abbreviated with a “p”). This results in the sample designation *SBA-15-ex-E-p* for SBA-15 with functionalized particle surface and open pores. To fix the metal complexes in the pores of SBA-15, the pore walls are modified. This step is abbreviated with “in” in the sample description. Since the concentration of the functional groups on the pore walls is adjusted by the reaction time, the reaction time is also listed. SBA-15, which has a functionalized external surface, opened pores and whose pore walls have been functionalized for 72 h is named *SBA-15-ex-E-p-in72*. Afterwards, linkers are attached to the functional groups on the pore walls to fix the metal complex for catalysis. The sample names with inserted linker carry the abbreviation of the alkyne. This results in *SBA-15-ex-E-p-in72-2c*, for example. Finally, the Rh complex is added which leads to the designation *SBA-15-ex-E-p-in72-2c*, $[\text{RhCl}(\text{C}_2\text{H}_4)_2]$. As reference materials, SBA-15 with metal complex exclusively on the external surface and with closed pores as well as SBA-15 with the metal complex attached on the particle surface and on the pore walls are used. They are called *SBA-15-ex-2c*, $[\text{RhCl}(\text{C}_2\text{H}_4)_2]$ and *SBA-15-ex+in-2c*, $[\text{RhCl}(\text{C}_2\text{H}_4)_2]$. The precursor of *SBA-15-ex-2c* is SBA-15 with azido groups exclusively on the external surface (*SBA-15-exN₃*).

Stepwise functionalization and characterization of SBA-15

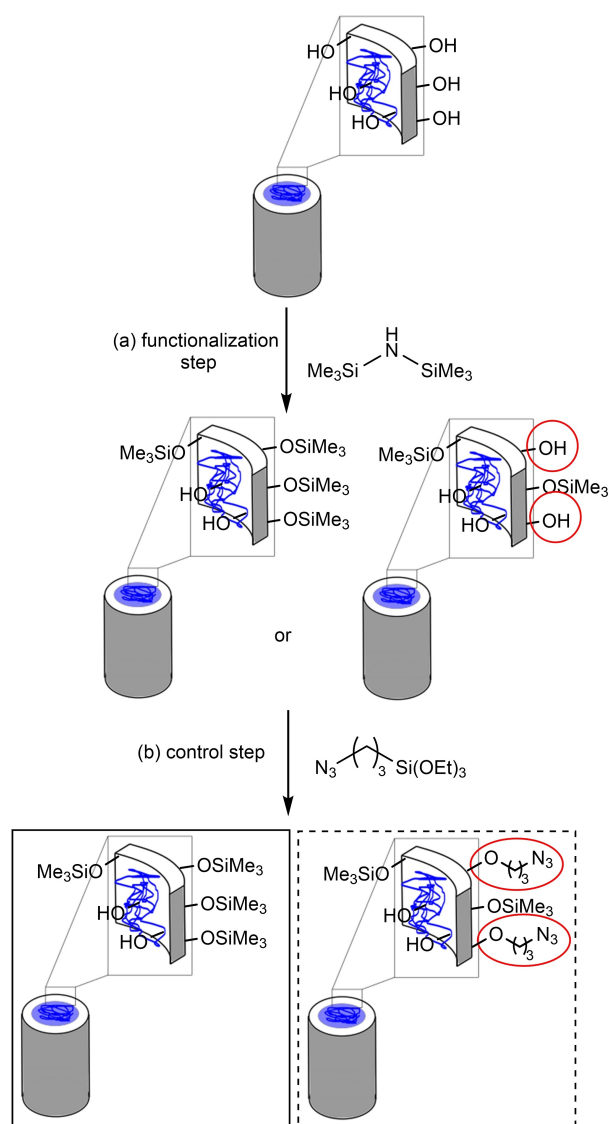
Functionalization of the particle surface and the pore mouths. The functionalization of the particle surface is important to ensure that the azide groups required for anchoring the catalyst complexes are located exclusively on the mesopore walls. The fact that the functionalization of the particle surface also



Scheme 2. Assignment of the sample names to a schematic representation of the corresponding material.

modifies the pore entrances and parts of the pore walls does not cause problems and is even desirable for the application described here, because an unambiguous confinement effect can only be studied if the catalyst is not located in close proximity of the pore entrance. Thus, it is more important to localize the azide groups, which are introduced in the functionalization step (Scheme 1, Step 3). To ensure that the particle surface and the pore mouths of the SBA-15 are fully functionalized and chemically inert during the second function-

alization step, we developed a method, which is shown schematically in Scheme 3. First, the particle surface as well as the pore mouths are functionalized (Scheme 3, (a) functionalization step). The as-synthesized SBA-15 with supposedly fully inert particle surface is then modified with AzPTES to control the inertization of the particle surface (Scheme 3, (b) control step). If the particle surface is inert or, more specifically, there are no accessible silanol groups left on the particle surface and the pore mouths, it will be impossible for AzPTES molecules to bind to the surface. This leads to the conclusion that the accessible silanol groups of the as-synthesized SBA-15 are completely modified or rather inert (Scheme 3, solid box). If the particle surface is not completely inert, there are still accessible silanol groups on the particle surface before the control step. These silanol groups are consequently functionalized in the control step with AzPTES. The attached azide groups can be



Scheme 3. Schematic description of the inertization of the particle surface and the pore mouths consisting of (a) a functionalization step and (b) a control step.

detected spectroscopically or by elemental analysis. The presence of azide groups on the particle surface would allow for the conclusion that the inertization of the particle surface was incomplete before the control step (Scheme 3, dashed box).

To verify if there are accessible silanol groups left on the particle surface or not, all compounds shown in Scheme 3 were investigated by means of IR spectroscopy. The IR spectrum of SBA-15 functionalized with HMDS (SBA-15-ex) in Figure 1 shows the characteristic bands of the silica between 1100 and 1000 cm^{-1} as well as between 800 and 729 cm^{-1} .^[30,31] Additionally, the characteristic bands of the silanol groups on the surface of SBA-15 are visible between 3550 and 2700 cm^{-1} and between 1010 and 832 cm^{-1} .^[30,31] However, it should be noted that the bands of the silanol groups are reinforced by adsorbed water molecules on the surface. The bands in the range between 2970 and 2850 cm^{-1} , at 1475 cm^{-1} and at 1375 cm^{-1} are due to CH_3 and CH oscillations.^[30–33] They are assigned to the structure-directing triblock copolymer P123 and the CH_3 groups on the particle surface which were introduced by functionalizing the particle surface with HMDS. Based on the IR spectrum, it is therefore impossible to make a statement as to whether the particle surface has been completely inertized in the functionalization step (Scheme 3(a)). Thus, the supposedly fully inertized SBA-15 (SBA-15-ex) was subjected to the control step with AzPTES (SBA-15-ex-control) (Scheme 3(b)). The IR spectrum of SBA-15 after the control step shows no differences to the IR spectrum of SBA-15-ex. This means that the usually intense band at 2100 cm^{-1} which is characteristic for azide groups is not visible.^[34] Because of this, it can be concluded that the silanol groups on the particle surface and in the pore entrances were completely functionalized with HMDS in the functionalization step (Scheme 3(a)). The binding of a surplus aza functionality is not possible, which is the prerequisite for the unambiguous binding of a complex to the inner mesopore wall (Scheme 1, Steps 3–5). Thus, the particle surface is inert

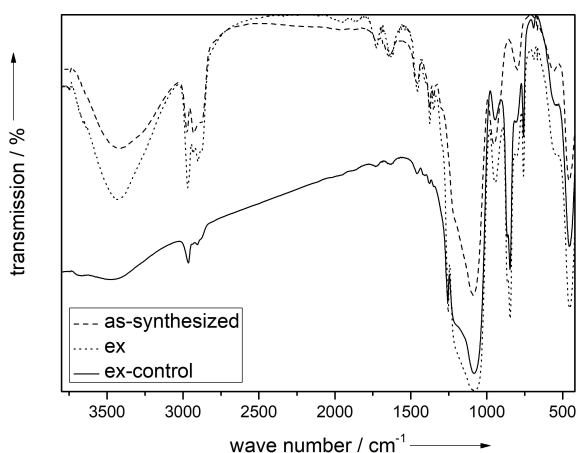


Figure 1. IR spectra of as-synthesized SBA-15 (dash), of SBA-15 after the functionalization step with HMDS (SBA-15-ex; dot) and of SBA-15 with functionalized particle surface after the control step (SBA-15-ex-control; solid) to check if the particle surface of the SBA-15 is completely inertized after the functionalization step of Scheme 3.

with respect to the functionalization of the pore walls. The results of the elemental analysis confirm the fact that the particle surface of SBA-15-ex is inert, since no nitrogen was detected in the sample SBA-15-ex-control (Table S2). The results from N_2 physisorption show that the functionalization with HMDS increases the BET surface and the pore diameter as compared to the as-synthesized material (Table 1). The HMDS treatment removes P123 from the particle surface and the pore mouths. The measurement gives not the real, cylindrical pore diameter (the pores are still filled with P123), but the larger diameter of the spherical or elliptical pore mouth.

Functionalization of the pore walls. After the inertization of the particle surface of the SBA-15 but before the functionalization of the pore walls, it is necessary to remove the structure-directing triblock copolymer P123 by Soxhlet extraction with ethanol (SBA-15-ex-E). The results from the N_2 physisorption measurements show that the treatment with ethanol removed a large part of the triblock copolymer P123 and leads to an increase of the total surface and pore volume compared to the SBA-15 with functionalized particle surface (SBA-15-ex) (Tables 1 and S1). Nevertheless, compared to the calcined SBA-15, the total surface and the pore volume remain smaller. The reason for this is that extraction with ethanol does not completely remove the triblock copolymer from the pores. By contrast, the pore diameter of extracted SBA-15 (SBA-15-ex-E) obtained from N_2 physisorption measurements is larger compared to the calcined SBA-15 (additional information in Table S1; isotherms of N_2 physisorption measurements and pore size distributions are shown in Figures S5 and S6). The difference can be explained by the fact that extraction of the triblock copolymer P123 with ethanol prevents the pores from shrinking. This effect of the shrinkage of the pores due to the calcination is described in the common literature.^[5] After the removal of the triblock copolymer P123 from the pores, the extracted SBA-15 was heated in a N_2 stream at 400 °C for 6 h (SBA-15-ex-E-p). This pretreatment leads to a shrinkage of the lattice parameter from 12.6 nm for SBA-15-ex to 11.7 nm for SBA-15-ex-E-p as shown by X-ray analysis (Table 1). The results are confirmed by N_2 physisorption measurements. The calculated pore diameter based on the physisorption isotherm is reduced by 0.28 nm to 7.31 nm due to the pretreatment in N_2 (Table 1). It was demonstrated with thermogravimetry and dynamic differential calorimetric studies that the N_2 pretreatment removed the last parts of the template remaining after Soxhlet extraction (SI, chapter 2). In addition, it could be shown that the functionalization of the external surface was stable during N_2 pretreatment at 400 °C (SI, chapter 2). The pretreatment ensured also that the silanol groups on the pore walls are in the more reactive geminal or single state and do not interact with each other via hydrogen bonds.^[35]

The influence of the type of silanol groups present on the surface on the functionalization was investigated with experiments performed on pretreated SBA-15 with only easily accessible (single and geminal) silanol groups (SBA-15-ex-E-p-in6) and on SBA-15 without pretreatment which had also interacting silanol groups (SBA-15-ex-E-in6). IR spectroscopic investigations of SBA-15-ex-E-in6 show no characteristic band in

the range of the expected band of the azide groups. By contrast, the IR spectrum of SBA-15, which was pretreated and subsequently functionalized with AzPTES (SBA-15-ex-E-p-in6), shows the band typical for azide groups at 2100 cm^{-1} (Figure 2). Consequently, the silanol species on the surface have an influence on whether azide groups can be attached to the surface or not. These results are confirmed by the results of the elemental analysis, which are listed in Table 1. The pore walls of the not pretreated sample (SBA-15-ex-E-in6) were not functionalized within 6 h, while the pretreated SBA-15-ex-E-p-in6 has an azide concentration of $3.41 \cdot 10^{-2}\text{ mmol g}^{-1}$ (Table 1). These results make clear that N_2 pretreatment of SBA-15 is necessary. It must also be considered that heating in N_2 leads to the opening of further pores of the SBA-15. The results of the N_2 physisorption measurements of SBA-15-ex-E-in6 and SBA-15-ex-E-p-in6 listed in Table 1 (additional information in Table S1; isotherms of N_2 physisorption measurements and pore size distributions are shown in Figures S5–S10) show that the non-pretreated SBA-15 has no micropores, whereas the SBA-15 (SBA-15-ex-E-p-in6) heated to 400°C in a N_2 stream has micropores. Generally, micropores lead to an increased BET surface and a decreased average pore diameter.

For varying the concentration of azide groups on the pore walls, the pretreated SBA-15-ex-E-p was functionalized with AzPTES at 80°C for a time period between 6 h and 72 h. The IR spectra of the SBA-15 with inert particle surface and with azide groups on the pore walls show the characteristic bands of the silica, the CH_3 groups on the particle surface and the oscillation band of the azide groups at 2100 cm^{-1} independent of the reaction time (Figure S50). A statement about the influence of the reaction time of the functionalization with AzPTES on the concentration of the azide groups attached to the pore walls cannot be made from IR spectroscopy since this is a qualitative method. For the investigation of the influence of the reaction time on the concentration of azide groups attached to the pore walls, the results of the elemental analysis were used (Table S2).

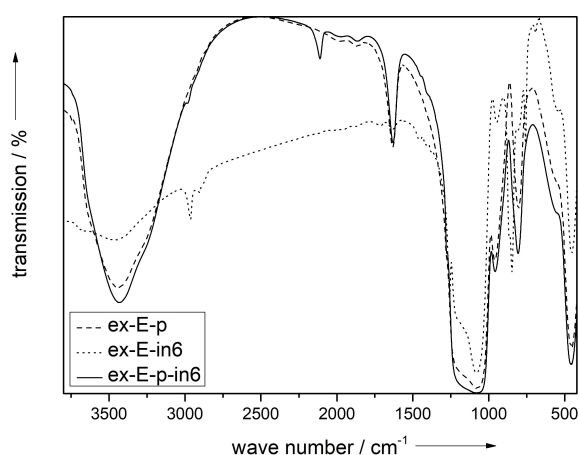


Figure 2. IR spectrum of SBA-15 with mesopores functionalized with AzPTES without N_2 pretreatment (SBA-15-ex-E-in6; dot) and with N_2 pretreatment (SBA-15-ex-E-p-in6; solid). As reference, the IR spectrum of SBA-15 after N_2 pretreatment without mesopore functionalization (SBA-15-ex-E-p; dash) is inserted.

Based on these results, the concentrations of the azide groups of the individual samples present on the pore walls per gram sample were calculated. The calculations give after a reaction time of 6 h $3.41 \cdot 10^{-2}\text{ mmol g}^{-1}$ azide groups, after 24 h $8.96 \cdot 10^{-2}\text{ mmol g}^{-1}$ and after 72 h $1.23 \cdot 10^{-1}\text{ mmol g}^{-1}$ (Table 1). The calculated concentrations show that with increasing reaction time more azide groups are present on the pore walls. Since the same amount of AzPTES was used for all experiments, it can be assumed that the influence of the reaction time on the concentration of the azide groups is due to the diffusion of AzPTES into the pores.

Further investigations concerning the amount of azide groups were performed by ^{13}C cross polarization (CP) MAS NMR spectroscopy with SBA-15-ex-E-p-in6 and SBA-15 whose external particle and internal mesopore surface was functionalized with AzPTES (SBA-15-ex+in). SBA-15-ex-E-p-in6 contains an azide concentration of $3.41 \cdot 10^{-2}\text{ mmol g}^{-1}$ while SBA-15-ex+in has an azide concentration of $2.03 \cdot 10^{-1}\text{ mmol g}^{-1}$. The two obtained ^{13}C spectra are shown in Figure 3. In both spectra, the signals of the azidopropyl moiety at 9 ppm, 22 ppm and 54 ppm can be observed. In addition, signals at a chemical shift $\delta_{13\text{C}} = 16\text{ ppm}$ and 59 ppm can be seen. They can be assigned to the ethoxy silane moieties that did not react with silanol groups on the surface.^[35,36] In principle, it is possible that AzPTES can react with up to three free silanol groups on the surface. If only one or two of the ethoxy groups react, the unreacted ethoxysilane moieties are visible in the ^{13}C CP MAS NMR spectrum. Furthermore, the spectrum of SBA-15-ex-E-p-in6 shows a strong signal at a chemical shift of $\delta_{13\text{C}} = -3\text{ ppm}$. It can be assigned to the $(\text{CH}_3)_3\text{-Si}$ moiety on the particle surface of the SBA-15.^[32] Overall, it is found that the intensities of all signals are relatively low which can be explained by the low concentration of functional groups on the surface and the absence of ^{13}C enrichment. A reason for the different signals observed are primarily the different functional groups present. On SBA-15-ex+in, only the azidopropyl moiety is found, while

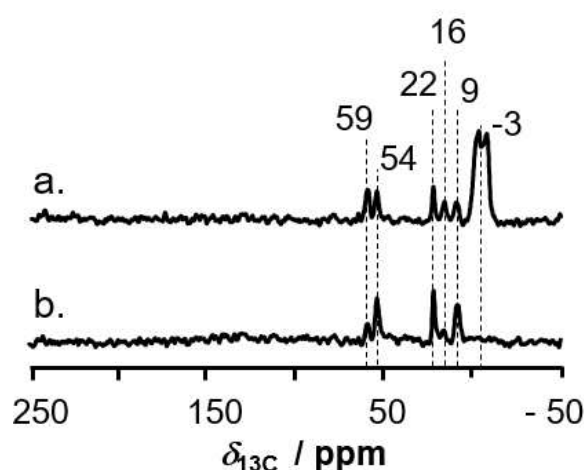


Figure 3. ^{13}C CP MAS NMR spectra of SBA-15, which only has azide groups in the mesopores (SBA-15-ex-E-p-in6; a.) and of SBA-15 which has azide groups on the external particle surface and on the walls of the mesopores (SBA-15-ex+in; b.).

on the surface of SBA-15-ex-E-p-in6, there are also $(\text{CH}_3)_3\text{-Si}$ moieties. Another reason is that the functional groups are present in different conformations on the surface. It is possible that the azidopropyl moiety protrudes into the pore at an angle of 90° to the pore wall. On the other hand, it is also conceivable that the azidopropyl moiety interacts with the pore walls and thus “rests” on them. Since the cross polarization intensity depends on the number of ^1H in close proximity to ^{13}C atoms, dynamics of the complexes and distances in between nuclei and the different conformations on the surface might result in different intensities of signals in the CP spectra.^[37] It can be summarized that the presence of the functional groups can be detected by ^{13}C CP MAS NMR spectroscopy. For reasons indicated above, a quantitative statement regarding the concentration of the functional groups is not possible. Furthermore, no statement can be made with this characterization method regarding the location of the functional groups. However, due to the applied functionalization procedure, the results show that the passivation of the particle surface stays intact after extraction and pretreatment. The location of the attached Rh complex is studied in a later section of this publication.

Besides the influence of the reaction time on the amount of azide groups, it was investigated whether the functionalization of the pore walls with azide groups influences the structure of the SBA-15. The total surface areas S_{BET} of the selectively functionalized SBA-15, determined from the isotherms of the N_2 physisorption measurements, are in a similar range as the total surface area of SBA-15 whose pore walls are not functionalized (SBA-15-ex-E-p) (Table 1). The same applies to the external and micropore surfaces. However, the observation of the pore volumes shows that the total pore volume increases with increasing azide concentration at the pore walls. The proportion of micropore volume does not show any dependence on the azide concentration (Table S1). A change of the pore diameter is not observed due to the functionalization of the pore walls with AzPTES (additional information in Table S1; isotherms of N_2 physisorption measurements and pore size distribution are shown in Figures S9 and S10). It can be concluded that the functionalization of the pore walls with AzPTES has no influence on the structure of the SBA-15, and the hexagonal arrangement of the pores is preserved. In addition to the N_2 physisorption measurements, TEM images were made of the intermediate stages of the SBA-15. The TEM images are shown in the supporting information and show no difference due to the functionalization (Figure S17–S20). Based on the TEM images, it is not possible to make a statement regarding the functionalization of the SBA-15. However, they show that the functionalization of the particle surface and the pore entrances, the removal of the template and the pretreatment, as well as the functionalization of the pore walls with AzPTES and the application of the metal complexes have no influence on the hexagonal structure.

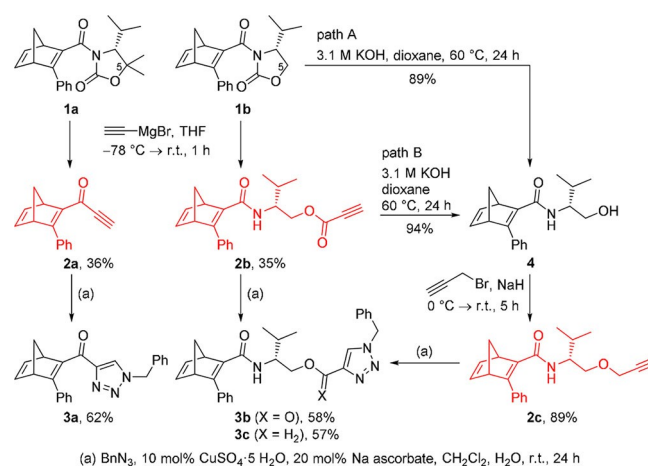
Synthesis of chiral diene ligands and their immobilization on SBA-15

In order to test the influence of the linker between diene ligand and mesoporous materials, three different chiral norbornadienes **2a–c** with terminal alkyne suitable for click immobilization were envisioned. As outlined in Scheme 4, the synthesis of norbornadienes **2** commenced with the treatment of known oxazolidinone-substituted 3-phenylnorbornadiene ligands **1a**, **b**^[38] with ethynyl magnesium bromide. Depending on the substitution pattern at C 5 of the oxazolidinone auxiliary (CMe_2 vs CH_2), either the propargylic ketone **2a** was obtained by exocyclic cleavage from **1a** or the tethered amide **2b** was isolated from **1b**. Saponification of **2b** to alcohol **4** and subsequent Williamson etherification^[39] with propargylic bromide yielded the respective propargylic ether **2c** in 89% yield (Scheme 4, path B). Alternatively, starting diene ligand **1b** was directly treated with KOH in dioxane to give alcohol **4**, which was etherified to **2c** (Scheme 4, path A).

For comparison of immobilized ligands **2** in heterogeneous catalysis with homogeneous catalysis, soluble triazole-containing ligands **3** were then prepared by reaction of **2a–c** with benzylazide in the presence of 10 mol% $\text{CuSO}_4 \cdot 5 \text{H}_2\text{O}$, 20 mol% Na ascorbate in CH_2Cl_2 and H_2O following a literature procedure.^[40] The click reaction of **2a**, **b** gave the respective triazoles **3a–c** in 57–62% yield.

With the ethynyl-tethered norbornadienes **2a–c** in hand, conditions for the click immobilization on SBA-15-ex+ in were screened. After some optimization, it was found that CuSO_4/Na ascorbate in $\text{CH}_2\text{Cl}_2/\text{H}_2\text{O}$ gave better results than $\text{CuI}/\text{iPr}_2\text{NET}$ in THF (Table S4) and that repetitive suspending/evaporation cycles improved the yield, presumably by overcoming diffusion problems. Under the optimized conditions, click immobilization of **2a** on various SBA-15 samples with different azide functionalization and azide loading was studied (Table 2).

As seen from Table 2, decreasing the azide concentration/loading in the mesopores significantly increased the conversion up to >99%. This result might be due to decreased steric



Scheme 4. Synthesis of alkyne-substituted norbornadienes **2a–c** and benchmark click reaction with benzylazide.

Entry	Alkyne	Azide functionalization ^[b]	Conc. N ₃ [mmol g ⁻¹]	t [d]	Conv. [%] ^[d]
1	2a	particle surface ^[c]	0.75	5	55
2	2a	particle surface + mesopores	0.75	3	46
3	2a	mesopores	0.19	3	78
4	2a	mesopores	0.17	3	72
5	2a	mesopores	0.10	3	> 99
6	2a	mesopores	0.06	3	> 99
7	2c	particle surface	0.085	3	80
8	2c	particle surface + mesopores	0.424	3	> 99
9	2c	mesopores	0.034	3	> 99
10	2c	mesopores	0.090	3	> 99
11	2c	mesopores	0.123	3	> 99

[a] Conditions: 1.5 eq. CuSO₄·5 H₂O, 3 eq. Na ascorbate, CH₂Cl₂, H₂O, r.t., [b] Materials dried under vacuum, [c] Without drying under vacuum, [d] Conversion of the alkyne determined from the ¹H NMR of the supernatant using mesitylene as the external standard.

hindrance of the azide groups inside the mesopores with decreasing concentration. When norbornadiene ligand **2c** with a more flexible tether between diene and propargylic ether was employed in the click immobilization, 80% up to quantitative conversion to the silica materials SBA-15 was obtained (Entries 7–11). The immobilization was monitored by ¹³C CP MAS NMR spectroscopy, IR spectroscopy and ICP-OES measurements.

For the immobilizations of **2a** on the particle surface as well as on the particle surface and on the walls of the mesopores (Entries 1,2), the azide band almost completely disappeared after the click reaction, while only 46–55% conversion of the alkyne **2a** was observed in the ¹H NMR spectra of the supernatants (Figures S46, S51, S52). Since the azide concentration of these materials was determined from the amount of azide used in the post-functionalization, it was assumed that the azide loadings were overestimated. In literature, elemental analysis is a common method to determine the amount of azide groups on the surface of silica.^[41] Therefore, the azide concentrations were determined by elemental analysis (Entries 3–9) to use only the effectively required amount of alkyne for the click reaction in the present work. Nevertheless, the azide bands were still strongly visible in the IR spectra, while the ¹H NMRs of the supernatants showed up to >99% conversion of the alkynes **2a**, **c**, when the linkers were clicked inside the mesopores (Figure S47, S48, S53–S56, S53–S56, S59–S62). It is assumed that there are further azide groups on the pore walls. Despite the excess of azide groups, it was possible to perform catalytic experiments with the correct catalyst loadings because the concentration of norbornadienes on the support could be calculated directly from the conversion of alkynes **2a**, **c** in the click reaction. Due to the characteristic bands of the azide groups in the IR spectra of the clicked materials, it is not possible to say whether the click reaction actually took place or whether the ligands are adsorbed on the pore walls. Therefore, the materials were additionally examined by ¹³C CP MAS spectroscopy. The spectra of both samples are shown in Figure 4. Both show the signals of the azidopropyl moiety at 9 ppm, 22 ppm and 54 ppm. Additionally, the ¹³C spectrum of the unclicked SBA-15 (Figure 4 a.) shows the signals of the ethoxysilane moieties at δ_{13C} = 16 ppm and 59 ppm that did not react with silanol groups on the surface during the functional-

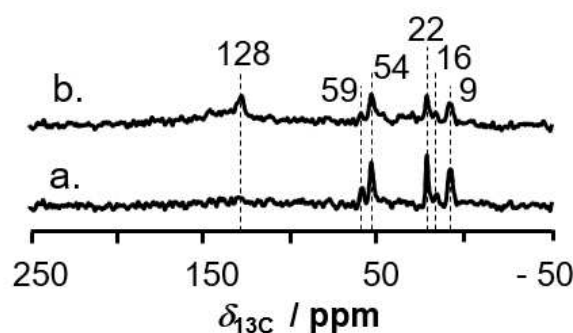


Figure 4. ¹³C CP MAS NMR spectra of SBA-15 which has azide groups on the external particle surface and in the internal mesopores (SBA-15-ex + in; a.) and of SBA-15 after the click reaction (SBA-15-ex + in-**2a**, b.).

ization step.^[23,32] Compared to the spectrum of the unclicked SBA-15 (SBA-15-ex + in), the ¹³C spectrum of the clicked SBA-15 (SBA-15-ex + in-**2a**) shows a signal at 128 ppm. It can be assigned to aromatic carbon atoms, for example in the triazole ring, which has a bond to a nitrogen atom and a double bond to another carbon atom.^[42] The presence of this signal suggests, that the click reaction was successful.

In the next step, Rh was immobilized on the materials. The amount of Rh applied was determined by ICP-OES analysis. The results show on the one hand that after the immobilization there is still Cu on the materials (Table S7). The Cu was needed for the click reaction. On the other hand, the results from elemental analysis show that around 60–80% of the Rh used in the immobilization interacts with the applied ligands (Table S7).

Investigation of the functionalization by scattering experiments

In addition to the verification of the hexagonal structure and the determination of the lattice parameters, we used small angle X-ray scattering (SAXS) to study the variation of the periodic electron density distribution due to the individual functionalization steps. This is possible as the square root of the scattered X-ray intensity *I* is proportional to the modulus of the

scattered wave $F(\mathbf{q})$, which is equal to the Fourier transform of the electron density $\rho(\mathbf{r})$ according to Equation (1):

$$\sqrt{I} \propto F(\mathbf{q}) = \int_V \rho(\mathbf{r}) \cdot \exp(2\pi i \mathbf{q} \cdot \mathbf{r}) d\mathbf{r} \quad (1)$$

with \mathbf{r} the spatial vector in real space and \mathbf{q} in reciprocal space, integrated over the probed volume V .^[43]

In Figure 5, the diffractograms of as-synthesized SBA-15 and solvent-extracted, pretreated SBA-15 (SBA-15-ex-E-p) are pictured. The peak positions shift to slightly larger q -values after the treatment with N_2 at 400°C , which causes a full condensation of the silica and thus a compacting of the structure. Additionally, a difference in the scattering intensities relative to the (100)-peak occurs, which is especially noticeable in the decrease of the intensity at q -values below 0.4 nm^{-1} and an increase above 0.8 nm^{-1} . This reflects the increased electron

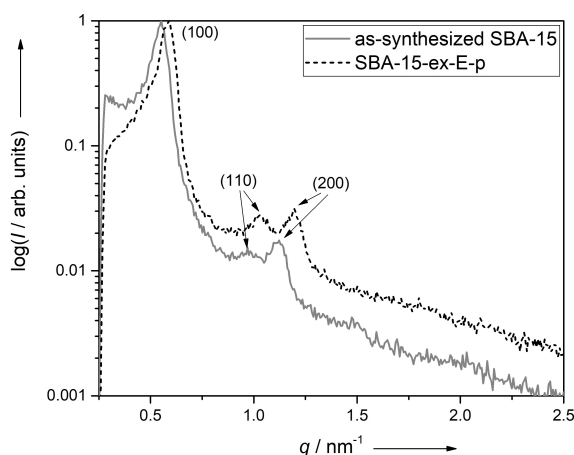


Figure 5. SAXS curves of the as-synthesized SBA-15 (solid) and the solvent-extracted and pretreated SBA-15 (SBA-15-ex-E-p; dash). The maximum scattering intensities, i.e., the (100)-peaks, are normalized to a value of 1 for better comparison.

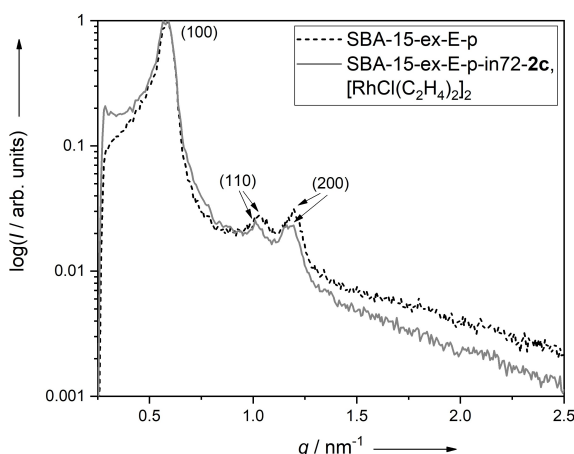


Figure 6. SAXS curves of SBA-15 functionalized with a Rh catalyst (SBA-15-ex-E-p-in72-2c, $[\text{RhCl}(\text{C}_2\text{H}_4)_2]_2$; solid) together with the one of the solvent-extracted SBA-15 (SBA-15-ex-E-p; dash).

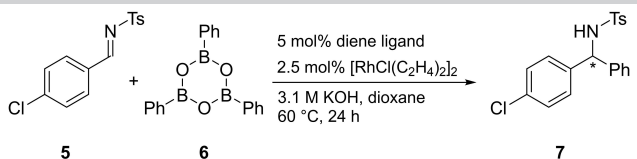
density contrast between the empty (air filled) pores and the silica walls compared to the pores filled with the template P123 and silica. Before extraction of the template but after the HDMS treatment, the relative intensity of the scattering curve can be found in between the two (Figure S21), which suggests that already during the HMDS treatment a part of the template is removed. It seems very unlikely that this change is due to the functionalization of the particle surface, considering that the average diameter of the particles is well above $0.1 \mu\text{m}$ and thus not accessible by SAXS measurements.

The subsequent functionalization steps all lead to gradual changes in the relative scattering intensity (Figures S22–S25) which is most prominent after the attachment of the electron-rich Rh catalyst. The scattering curve of the SBA-15 with the highest catalyst loading (SBA-15-ex-E-p-in72-2c, $[\text{RhCl}(\text{C}_2\text{H}_4)_2]_2$ $0.123 \text{ mmol g}^{-1}$) is depicted in Figure 6 together with the one of the ethanol-extracted SBA-15 (SBA-15-E-p). Compared to the extracted material, the diffractogram of the catalyst-containing material exhibits increased relative scattering intensities for small q -values and decreased ones above $q = 1 \text{ nm}^{-1}$. This makes it look more similar to the scattering curve of the as-synthesized SBA-15 and suggests that the electron density distribution of SBA-15-ex-E-p-in72-2c, $[\text{RhCl}(\text{C}_2\text{H}_4)_2]_2$ has been altered in a periodic manner, considering that non-periodic changes would cause no q -dependent changes of the scattered intensity. Additionally, by comparing the different catalyst loadings, it is also obvious that the change of the scattered intensity correlates with the concentration of the catalyst (Figure S24).

Thus, the decreasing electron density contrast after selective functionalization, identified by the similarities between the SAXS curves of complex-bearing SBA-15 and template-bearing as-synthesized SBA-15, indicates a functionalization in the pores. Combined with the absence of binding sites on the surface, as proven by IR spectroscopy, we conclude that the ligand was unambiguously immobilized to the mesopore wall.

Initial results in asymmetric Rh-catalyzed 1,2-additions under confinement

A first series of catalytic reactions was performed with SBA-15 functionalized with rigid triazolyl tether SBA-15-2a differing in their internal and particle surface functionalization and diene content (Table 3). For example, the addition of $2.5 \text{ mol}\%$ $[\text{RhCl}(\text{C}_2\text{H}_4)_2]_2$ to a suspension of SBA-15-ex-2a in dioxane in the presence of 3.1 M KOH to immobilize the Rh on the functionalized SBA-15 followed by addition of *N*-tosylimine **5** and triphenylboroxine **6** and heating at 60°C for 24 h gave the addition product *N*-tosylamine **7** in an isolated yield of 11% and enantioselectivity of 73:27 in favor of the (*R*) enantiomer (Entry 1). With SBA-15-ex+in-2a containing dienes at the internal mesopore surface and the particle surface (0.35 mmol g^{-1} of **3** on SBA-15), the NMR yield of **7** was disappointingly low (1%) (Entry 2). Upon use of SBA-15-ex-E-in24-2a, SBA-15-ex-E-p-in24-2a or SBA-

Table 3. Comparison of Rh-catalyzed 1,2-addition of phenylboroxine **6** to *N*-tosylimine **5** with immobilized catalysts and catalysts in solution.


Entry	Catalyst	Conc. of 3 on SBA-15 [mmol g ⁻¹]	NMR	Yield of 7 [%] isol.	E.r. R:S
1 ^[a]	SBA-15-ex- 2a , [RhCl(C ₂ H ₄) ₂] ₂	0.41	16	11	73:27
2 ^[a]	SBA-15-ex + in- 2a , [RhCl(C ₂ H ₄) ₂] ₂	0.35	1	n.d.	n.d.
3 ^[a]	SBA-15-ex-E-p-in72- 2a , [RhCl(C ₂ H ₄) ₂] ₂	0.19	1	n.d.	n.d.
4 ^[a]	SBA-15-ex-E-p-in24- 2a , [RhCl(C ₂ H ₄) ₂] ₂	0.15	1	n.d.	n.d.
5 ^[a]	SBA-15-ex-E-in72- 2a , [RhCl(C ₂ H ₄) ₂] ₂	0.12	traces	n.d.	n.d.
6 ^[a]	SBA-15-ex-E-in24- 2a , [RhCl(C ₂ H ₄) ₂] ₂	0.06	0	n.d.	n.d.
7 ^[a]	SBA-15-ex- 2c , [RhCl(C ₂ H ₄) ₂] ₂	0.068	8	n.d.	n.d.
8 ^[a]	SBA-15-ex + in- 2c , [RhCl(C ₂ H ₄) ₂] ₂	0.424	75	70	14:86
9 ^[a]	SBA-15-ex-E-p-in6- 2c , [RhCl(C ₂ H ₄) ₂] ₂	0.034	29	16	15:85
10 ^[a]	SBA-15-ex-E-p-in24- 2c , [RhCl(C ₂ H ₄) ₂] ₂	0.090	31	28	18:82
11 ^[a]	SBA-15-ex-E-p-in72- 2c , [RhCl(C ₂ H ₄) ₂] ₂	0.123	47	47	17:83
12 ^[b]	2a , [RhCl(C ₂ H ₄) ₂] ₂	–	58	40	82:18
13 ^[b]	3a , [RhCl(C ₂ H ₄) ₂] ₂	–	5	n.d.	n.d.
14 ^[b]	2c , [RhCl(C ₂ H ₄) ₂] ₂	–	91	81	20:80
15 ^[b]	2b , [RhCl(C ₂ H ₄) ₂] ₂	–	61	52	23:77
16 ^[b]	3b , [RhCl(C ₂ H ₄) ₂] ₂	–	80	69	15:85
17 ^[b]	3c , [RhCl(C ₂ H ₄) ₂] ₂	–	62	58	19:81
18	[RhCl(C ₂ H ₄) ₂] ₂	–	5	n. d.	n. d.

[a] The catalysts for heterogeneous catalysis were prepared by addition of 2.5 mol% [RhCl(C₂H₄)₂]₂ to a suspension of 5 mol% immobilized diene ligand in dioxane, subsequent stirring for 30 min at room temperature and addition of 3.1 M KOH, [b] The catalysts for homogeneous catalysis were prepared by addition of 2.5 mol% [RhCl(C₂H₄)₂]₂ to a solution of 5 mol% diene ligand in dioxane subsequent stirring for 15 min at room temperature and addition of 3.1 M KOH.

15-ex-E-p-in72-**2a** and decreasing the diene content, the yields could not be improved (Entries 3–6). Homogeneous catalysis with alkyne- (**2a**) and triazolyl-containing **3a** was performed for comparison. Diene **2a** led to **7** in 40% isolated yield with a slightly higher enantiomeric (*R*):(*S*) ratio of 82:18 (Entry 12). By contrast, diene **3a** gave only 5% NMR conversion. These results suggest that the triazole in close proximity to the diene unit suppresses the Rh catalysis, presumably due to electronic interference of the triazolyl moiety with the Rh center and steric hindrance exerted inside the mesopore.

We surmised that the ligand **3c** with a more flexible tether between diene and triazole unit might be better suited for heterogeneous catalysis. As shown in Table 3, Rh-catalyzed 1,2-addition using externally functionalized SBA-15-ex-**2c** (0.068 mmol g⁻¹ of **3** on SBA-15) only yielded 8% *N*-tosylamine **7** (Entry 7). When the immobilized diene SBA-15-ex + in-**2c** with additional functionalization inside the mesopores and the highest diene content (0.424 mmol g⁻¹ of **3** on SBA-15) was used the yield was significantly increased to 75% and an (*R*):(*S*) ratio of 14:86 was obtained (Entry 8). Internally functionalized SBA-15-ex-E-p-in6-**2c** (0.034 mmol g⁻¹ of **3** on SBA-15) yielded 16% *N*-tosylamine **7** with an (*R*):(*S*) ratio of 15:85 (Entry 9). Higher diene content slightly decreased the enantiomeric ratio to 17:83, but improved the yield (47%, Entry 11). It should be noted that the material SBA-15-ex-**2c** carrying diene ligands only at the external surface gave only a very poor yield (8%, Entry 7). Thus, despite the better steric accessibility of the external surface-bound ligands, a higher catalytic activity was determined inside the mesopores. For comparison, the addition

reaction was run with soluble dienes. Norbornadienes **2b** and **2c** gave higher yields but slightly lower enantioselectivities, whereas **3b** with acyltriazolyl moiety gave **7** in 69% yield with an enantiomeric ratio of 15:85 (Entries 14–17). When **3c** was applied, the *N*-tosylamine **7** was obtained in 58% yield with an enantiomeric ratio of 19:81 (Entry 17). This is in good agreement with the results obtained for the immobilized ligand (Entries 7–11). The results indicate that the triazole unit in the spacer does not disturb the Rh catalysis as long as it is kept at distance and the spacer has some conformational flexibility. To investigate whether background catalysis of the rhodium precursor takes place, an experiment with only [RhCl(C₂H₄)₂]₂ and no diene ligand was carried out (Entry 18). Only 5% yield of *N*-tosylamine **7** was observed and therefore it can be concluded that background catalysis of the precursor is insignificant.

Since high concentrations of copper were detected on the immobilized systems via ICP-OES, a series of experiments with addition of CuSO₄·5 H₂O was done to secure that copper species do not disturb the 1,2-addition (Tables S8 and S9). We found that copper neither in homogeneous nor in heterogeneous catalysis had a significant impact on yield and enantioselectivity. Furthermore, SBA-15-ex-E-p-in72-**2c** was washed several times with EDTA solution and then applied in catalysis for comparison (Table S9). The results were similar to the results obtained with the non-washed supported catalyst.

In addition to the investigations on catalysis, investigations on the leaching of the Rh from the SBA-15 were carried out. For this purpose, the SBA-15, which was recovered after catalysis, and the supernatant of the catalysis were investigated by ICP-

OES. The results show that small amounts of Rh are present in the supernatant (Table S6). However, small amounts of Si of SBA-15 are also found (Table S5). It is assumed that the Rh is still present on the SBA-15. An explanation for the small amounts of catalyst in the supernatant is that during the reaction, due to the reaction conditions (e.g., strong stirring), tiny particles of the mesoporous support material are removed by abrasion together with the catalyst immobilized on it. Due to their small particle size, they cannot be recovered by centrifugation during separation. This means that no leaching occurred during the experiments (Table S5 and S6).

Furthermore, it was tested whether the immobilized diene ligand leaches into solution under the basic conditions of the catalysis. Thus, the supernatant from the catalysis with SBA-15-ex-E-p-in72-2c was filtered through a filter paper and the filtrate measured via ESI-MS (Figure S62). Since no peak in the mass spectrum could be assigned to the diene ligand or any hydrolysis fragment, it was assumed that no leaching of the ligand occurs. Finally, the recyclability of the immobilized system SBA-15-ex-E-p-in72-2c was tested (Table S10). For the first and the second cycle, similar yields and enantioselectivities were observed. After the third cycle, the yield significantly decreased. Therefore, fresh $[\text{RhCl}(\text{C}_2\text{H}_4)_2]_2$ was added to the catalyst and a fourth cycle was tested. Unfortunately, the yield could not be improved and thus it was assumed that the catalyst irreversibly deactivated in agreement with results by Yang and Xu on A–B type sterically regular polymeric 2,4-diphenylbicyclo[3.3.0]octadienes.^[44]

Conclusions

In this work, we present a method for the efficient and spatially controlled functionalization of SBA-15. First, the silanol groups on the particle surface and in the pore entrances were passivated with 1,1,1-trimethyl-*N*-(trimethylsilyl)silanamine. After extraction of the structure-directing agent Pluronic® P123 with ethanol, a pretreatment step at 400 °C in N₂ converted the silanol groups to the single and geminal state. Afterwards, the azide functionality was introduced *exclusively* into the mesopores. This could be shown by use of a control step and characterization by SAXS. Therefore, the Rh-containing catalyst could be immobilized *unambiguously* in the mesopores. Initial catalytic asymmetric Rh-catalyzed 1,2-additions revealed that the linker between catalyst and pore wall played an important role in the heterogeneous catalysis. While short rigid triazole-containing linkers completely suppressed the conversion of *N*-tosylimines to the corresponding amines, longer and more flexible linkers did not interfere with the catalysis. Comparison with the corresponding soluble catalysts under homogeneous conditions revealed that the triazole unit is an innocent ligand as long as it is sufficiently far away positioned from the Rh catalyst, resulting in good yields and enantioselectivities. Thus, future experiments need to investigate confinement effects resulting from the interplay of pore size, pore geometry and linker lengths on the enantioselective heterogeneous catalysis.

Work along these lines is currently in progress in our laboratories.

Experimental Section

Synthesis of SBA-15. For the synthesis of SBA-15, 16 g of triblock copolymer Pluronic P123 (average molar mass $\sim 5800 \text{ g mol}^{-1}$, Sigma Aldrich) was dissolved in a mixture of 520 ml demineralized water and 80 ml 37 wt% hydrochloric acid at room temperature and a stirring speed of 100 rpm overnight. The solution was heated to 45 °C before adding 37 ml tetraethyl orthosilicate (TEOS, 98%, reagent grade, Sigma Aldrich). The mixture was stirred for 7.5 h at 45 °C with a stirring speed of 150 rpm. A hydrothermal treatment under static conditions at 80 °C followed. Afterwards, the as-synthesized SBA-15 was separated under vacuum, washed with demineralized water and dried in an oven at 80 °C. To open the pores, the as-synthesized SBA-15 was calcined at 550 °C in an air flow of 150 l h^{-1} . The heating rate was 1 K min^{-1} .

Functionalization of the particle surface and the pore mouths. The functionalization of the particle surface of as-synthesized SBA-15 was performed in pure 1,1,1-trimethyl-*N*-(trimethylsilyl)silanamine (HMDS, $\geq 98\%$ (for GC), Carl Roth GmbH + Co. KG). The suspension of HMDS and as-synthesized SBA-15 was stirred at room temperature for 6 h. The functionalized material (SBA-15-ex) was separated under vacuum, washed with demineralized water and dried in an oven at 80 °C.

Removal of P123. The triblock copolymer P123 was removed from the pores of the SBA-15-ex by Soxhlet extraction over 112 h using ethanol as extracting agent. The extracted material (SBA-15-ex-E) was dried in an oven at 80 °C.

Pretreatment before the functionalization of the internal surface. Before the functionalization of the pore walls took place, SBA-15-ex-E was treated in an oven at 400 °C for 6 h in N₂. The treatment was performed with a heating rate of 2 K min^{-1} and a nitrogen flow of 58 l h^{-1} . The product obtained was named SBA-15-ex-E-p.

Functionalization of the internal surface. A suspension of 15 ml toluene and $9.5 \cdot 10^{-4} \text{ mol}$ 3-azidopropyltriethoxysilane (AzPTES, prepared after Nakazawa et al.^[45]) per gram SBA-15-ex-E-p was prepared to functionalize the pore walls. The reaction mixture was stirred at room temperature. The reaction time was between 6 h and 72 h to vary the concentration of the azide moieties on the pore walls. The functionalized SBA-15 (SBA-15-ex-E-p-in) was separated under vacuum, washed with ethanol and dried in the oven at 80 °C.

Copper-catalyzed azide-alkyne cycloadditions with SBA-15. To a suspension of the azide-functionalized SBA-15 (e.g., 0.60 g, $54.0 \mu\text{mol}$ azide, $c_{\text{N}_3} = 0.09 \text{ mmol g}^{-1}$) in CH₂Cl₂ (5 mL), a solution of the alkyne 2c (18.1 mg, $54.0 \mu\text{mol}$) in CH₂Cl₂ (181 μL) was added. The solvent was evaporated under reduced pressure, and CH₂Cl₂ (6 mL) was added. This step was repeated twice. Degassed water (6 mL), sodium ascorbate (31.7 mg, 0.16 mmol) and CuSO₄·5 H₂O (10.1 mg, 40.5 μmol) were added, and the reaction mixture was stirred for 2 d at room temperature in the dark. CuSO₄·5 H₂O (10.1 mg, 40.5 μmol) was added, and the reaction mixture was stirred for another 24 h at room temperature. The dispersion was centrifuged with 4000 rpm, the sediment was washed with CH₂Cl₂ (4 mL) and the suspension was centrifuged again. The sediment was washed with water (4 mL), centrifuged and washed with EtOAc (4 mL). After an additional centrifugation step, the sediment was dried under vacuum, and the diene-functionalized material was obtained as a colorless solid (0.44 g, $\geq 99\%$ alkyne conversion, 0.09 mmol/g 3c). For the determination of the conversion of 2c,

the combined supernatants were extracted with CH_2Cl_2 (3×10 mL), the combined organic layers were dried over MgSO_4 , and the solvent was removed under reduced pressure. The residue was taken up in CDCl_3 (0.4 mL) and the conversion of **2c** was determined from the ^1H NMR spectrum using mesitylene (7.46 μL , 6.49 mg, 54.0 μmol) as the external standard.

Catalytic 1,2-additions with diene-functionalized SBA-15. $[\text{RhCl}(\text{C}_2\text{H}_4)_2]_2$ (e.g., 1.94 mg, 5.00 μmol) was added under a N_2 atmosphere to a suspension of the diene-functionalized material SBA-15-ex-E-p-in72-2c (81.3 mg, 10.0 μmol diene, $c(\text{diene}) = 0.123 \text{ mmol g}^{-1}$) in degassed dioxane (2.0 mL). The suspension was stirred for 30 min at room temperature, 3.1 M KOH (12.9 μL , 40.0 μmol) was added and the suspension was stirred for another 5 min at room temperature. The reaction mixture was heated to 60°C , triphenylboroxine **6** (74.8 mg, 0.24 mmol) and *N*-tosylimine **5** (58.8 mg, 0.20 mmol) were added, and the reaction mixture was stirred for 24 h at 60°C . EtOAc (2 mL) was added, the suspension was centrifuged with 4000 rpm and the solvent of the supernatant was removed under reduced pressure. The crude product was purified by column chromatography on silica (PE/EtOAc = 10:1), and the *N*-tosylamine **7** was obtained as a colorless solid (34.0 mg, 91.4 μmol , 47%).

Characterization methods

SAXS. The powdery samples were filled into mark capillaries with a diameter of 1 mm (Hilgenberg, glass no. 14) and flame-sealed. For measurements, a SAXSess mc^2 diffractometer (Anton Paar) in the line collimation geometry was used for which the sample to detector distance was calibrated with cholesteryl palmitate. X-ray radiation with a wavelength of $\lambda(\text{Cu-K}\alpha) = 0.1542 \text{ nm}$ was generated by an ID 3003 X-ray generator (Seifert) operated at 40 kV and 40 mA. To ensure a uniform irradiation of all lattice planes, samples were rotated during the measurement using a RotorCell placed in a TCS 120 hot stage (both Anton Paar). The sample housing was evacuated prior to measurements, which were carried out at 25°C and averaged over 60 individual measurements. The scattered X-ray intensity was detected with a one-dimensional CMOS Mythen 2 K detector (Dectris). Using the software SAXSquantTM, the measured scattering profiles were background corrected with a measurement of an empty mark capillary and deconvoluted. The obtained Bragg-like diffraction maxima were fitted with Lorentzian functions to extract the exact peak positions.

N_2 physisorption. The surface area as well as the pore size of the SBA-15 samples were analyzed by N_2 physisorption measurements. The adsorption and desorption isotherms were recorded using Autosorb 3B from Quantachrome Instruments. Before the measurements, the samples were outgassed under vacuum at 200°C for 16 h. After the pretreatment, the nitrogen physisorption measurements were performed in a liquid nitrogen bath at -196°C . From the adsorption isotherms, the surfaces were calculated using the BET method, whereas the pore sizes and pore size distributions were determined with the DFT method, taking into account the hexagonal structure.

FTIR. To characterize the functional groups on the surface of SBA-15, the samples were examined by IR spectroscopy. The spectrometer Nicolet 6700 from Thermo Scientific was used. The spectra were examined in the range from 3800 cm^{-1} to 420 cm^{-1} with 16 scans and a resolution of 4 cm^{-1} . For the measurements, tablets of potassium bromide (KBr for IR spectroscopy, Uvasol[®], Sigma Aldrich) and the sample were prepared. The mass ratio of KBr to the sample was 200.

Elemental analysis. The amount of carbon, hydrogen and nitrogen was measured with an Elemental Analyzer 1106 from the company

Carlo Erba Strumentazione. To determine the copper and rhodium content, the clicked samples and the samples after catalysis were analyzed by plasma-induced optical electron emission spectroscopy (ICP-OES). The analysis was performed on an Avio 200 of Perkin Elmer. In preparation for the measurement, the samples were digested with 3 mL 10% hydrofluoric acid and 3 mL aqua regia in a microwave oven up to 200°C and diluted with 3 mL aqua regia and demineralized water before the measurement.

Solid state NMR. ^1H - ^{13}C CP MAS NMR experiments were performed on an Avance III 400WB spectrometer at a resonance frequency of 100.6 MHz, at a spin rate of 8 kHz (in 4 mm rotors with Kel-F cap), using a contact time of 3 ms, a 70–100 ramp during the Hartmann-Hahn contact period and spinal64 decoupling during acquisition. A delay of 5 s between the scans was applied, at least 35000 scans accumulated (measurement time > 2 d) and the background subtracted. Spectra were referenced to adamantane at 38.48 ppm.

Acknowledgements

Funded by the Deutsche Forschungsgemeinschaft (DFG, German Research Foundation) – Project-ID 358283783-SFB 1333).

We would also like to thank Barbara Gehring and Claudia Lauxmann for carrying out the elemental analysis, Heike Fingerle for performing the ICP-OES measurements and Jan Florenski for doing the TG-DTA measurements. Open access funding enabled and organized by Projekt DEAL.

Conflict of Interest

The authors declare no conflict of interest.

Keywords: Asymmetric catalysis · Confinement · Rhodium · SBA-15 · Spatially controlled functionalization

- [1] C. T. Kresge, M. E. Leonowicz, W. J. Roth, J. C. Vartuli, J. S. Beck, *Nature* **1992**, *359*, 710–712.
- [2] V. Meynen, P. Cool, E. F. Vansant, *Microporous Mesoporous Mater.* **2009**, *125*, 170–223.
- [3] P. Alexandridis, T. Alan Hatton, *Colloids Surf. A* **1995**, *96* (1–2), 1–46.
- [4] D. E. de Vos, M. Dams, B. F. Sels, P. A. Jacobs, *Chem. Rev.* **2002**, *102*, 3615–3640.
- [5] a) F. Kleitz, W. Schmidt, F. Schüth, *Microporous Mesoporous Mater.* **2003**, *65*, 1–29; b) I. Mbaraka, B. Shanks, *J. Catal.* **2005**, *229*, 365–373.
- [6] M. Liong, S. Angelos, E. Choi, K. Patel, J. F. Stoddart, J. I. Zink, *J. Mater. Chem.* **2009**, *19*, 6251.
- [7] J. D. Webb, T. Seki, J. F. Goldston, M. Pruski, C. M. Crudden, *Microporous Mesoporous Mater.* **2015**, *203*, 123–131.
- [8] D. S. Shephard, W. Zhou, T. Maschmeyer, J. M. Matters, C. L. Roper, S. Parsons, B. F. G. Johnson, M. J. Duer, *Angew. Chem. Int. Ed. Engl.* **1998**, *37*, 2719–2723.
- [9] N. Linares, E. Serrano, M. Rico, A. M. Balu, E. Losada, R. Luque, J. García-Martínez, *Chem. Commun.* **2011**, *47*, 9024–9035.
- [10] V. Cauda, A. Schlossbauer, J. Keck, A. Zürner, T. Bein, *J. Am. Chem. Soc.* **2009**, *131*, 11361–11370.
- [11] a) T. Asefa, R. B. Lennox, *Chem. Mater.* **2005**, *17*, 2481–2483; b) F. de Juan, E. Ruiz-Hitzky, *Adv. Mater.* **2000**, *12*, 430–432.
- [12] F. Liu, J. Wang, P. Huang, Q. Zhang, J. Deng, Q. Cao, J. Jia, J. Cheng, Y. Fang, D. Y. B. Deng, W. Zhou, *J. Mater. Chem. B* **2015**, *3*, 2206–2214.
- [13] A.-H. Lu, W.-C. Li, A. Kiefer, W. Schmidt, E. Bill, G. Fink, F. Schüth, *J. Am. Chem. Soc.* **2004**, *126*, 8616–8617.

- [14] a) V. Antochshuk, A. S. Araujo, M. Jaroniec, *J. Phys. Chem. B* **2000**, *104*, 9713–9719; b) V. Antochshuk, M. Jaroniec, *Chem. Mater.* **2000**, *12*, 2496–2501.
- [15] N. Gartmann, D. Brühwiler, *Angew. Chem. Int. Ed. Engl.* **2009**, *48*, 6354–6356.
- [16] a) P. Alexandridis, R. Ivanova, B. Lindman, *Langmuir* **2000**, *16*, 3676–3689; b) J. Herzberger, K. Niederer, H. Pohlitz, J. Seiwert, M. Worm, F. Wurm, H. Frey, *Chem. Rev.* **2016**, *116*, 2170–2243; c) K. Mortensen, J. S. Pederson, *Macromolecules* **1993**, *26*, 805–812.
- [17] M. Dixit, M. Manish, P. A. Joshi, D. O. Shah, *Procedia Eng.* **2013**, *51*, 467–472.
- [18] A. Patel, P. Shukla, T. Rufford, S. Wang, J. Chen, V. Rudolph, Z. Zhu, *Appl. Catal. A* **2011**, *409–410*, 55–65.
- [19] a) C. M. Crudden, M. Sateesh, R. Lewis, *JACS* **2005**, *127*, 10045–10050; b) V. Polshettiwar, C. Len, A. Fihri, *Coord. Chem. Rev.* **2009**, *253*, 2599–2626.
- [20] S. Verma, M. Nandi, M. Mahasweta, J. Arindam, L. Suman, A. Bhaumik, *Adv. Synth. Catal.* **2011**, *353*, 1897–1902.
- [21] S. L. Jain, B. S. Rana, B. Singh, A. K. Sinha, A. Bhaumik, M. Nandi, B. Sain, *Green Chem.* **2010**, *12*, 374–377.
- [22] C.-M. Yang, H.-A. Lin, B. Zibrowius, B. Spliethoff, F. Schüth, S.-C. Liou, M.-W. Chu, C.-H. Chen, *Chem. Mater.* **2007**, *19*, 3205–3211.
- [23] F. Liu, J. Wang, P. Huang, Q. Zhang, J. Deng, Q. Cao, J. Jia, J. Cheng, Y. Fang, D. Y. B. Deng, W. Zhou, *J. Mater. Chem. B* **2015**, *3*, 2206–2214.
- [24] J. D. Webb, T. Seki, J. F. Goldston, M. Pruski, C. M. Crudden, *Micro- and Mesoporous Materials* **2015**, *203*, 123–131.
- [25] a) A. E. Fernandez, A. M. Jonas, O. Riant, *Tetrahedron* **2014**, *70*, 1709–1731; b) Y. Li, C. Cai, *Chem. Asian J.* **2011**, *6*, 2592–2605.
- [26] a) H. Ying, C. Cai, *Chem. Commun.* **2011**, *47*, 12319–12321; b) A. R. McDonald, N. Franssen, G. P. M. van Klink, G. van Koten, *J. Org. Chem.* **2009**, *694*, 2153–2162.
- [27] a) C. Defieber, H. Grützmacher, E. M. Carreira, *Angew. Chem. Int. Ed.* **2008**, *47*, 4482–4502; *Angew. Chem.* **2008**, *120*, 4558–4579; b) J. B. Johnson, T. Rovis, *Angew. Chem. Int. Ed.* **2008**, *47*, 840–871; *Angew. Chem.* **2008**, *120*, 852–884; c) C.-G. Feng, M.-H. Xu, G.-Q. Lin, *Synlett* **2011**, 1345–1356; d) X. Feng, H. Du, *Asian J. Org. Chem.* **2012**, *1*, 204–213.
- [28] a) T. Mühlhäuser, A. Savin, W. Frey, A. Baro, A. J. Schneider, H.-G. Döteberg, F. Bauer, A. Köhn, S. Laschat, *J. Org. Chem.* **2017**, *82*, 13468–13480; b) N. Sieffert, J. Boisson, S. Py, *Chem. Eur. J.* **2015**, *21*, 9753–9768; c) T. Yasukawa, T. Kuremoto, H. Miyamura, S. Kobayashi, *Org. Lett.* **2016**, *18*, 2716–2718; d) C. C. Chen, B. Gopula, J.-F. Syu, J.-H. Pan, T.-S. Kuo, P.-Y. Wu, J. P. Henschke, H.-L. Wu, *J. Org. Chem.* **2014**, *79*, 8077–8085; e) Y. Luo, H. B. Hepburn, N. Chotsaeng, H. W. Lam, *Angew. Chem. Int. Ed.* **2012**, *51*, 8309–8313; *Angew. Chem.* **2012**, *124*, 8434–8438; f) T. Nishimura, T. Nagai, R. Takechi, Y. Ebe, *Synthesis* **2016**, *48*, 2612–2618; g) F. Xue, Q. Liu, Y. Zhu, Y. Qing, B. Wan, *RSC Adv.* **2019**, *9*, 25377–25381.
- [29] M. Deimling, M. Kirchhof, B. Schwager, Y. Qawasmi, A. Savin, T. Mühlhäuser, W. Frey, B. Claasen, T. Sottmann, S. Laschat, *Chem. Eur. J.* **2019**, *25*, 9464–9476.
- [30] G. F. Andrade, D. C. Soares, R. Almeida, E. Sousa, *J. Nanomater.* **2012**, *1*, 1–10.
- [31] D. Liu, J.-H. Lei, L.-P. Guo, K. Zeng, *Microporous Mesoporous Mater.* **2009**, *117*, 67–74.
- [32] A. Feliczek-Guzik, B. Jadach, H. Piotrowska, M. Murias, J. Lulek, I. Nowak, *Microporous Mesoporous Mater.* **2016**, *220*, 231–238.
- [33] M. Hesse, H. Meier, B. Zeeh in *Spektroskopische Methoden in der organischen Chemie, 7. Überarb. Aufl.*, Georg Thieme Verlag KG, Stuttgart, **2005**, pp. 40–56.
- [34] B. Malvi, B. R. Sarkar, D. Pat, R. Mathew, T. G. Ajithkumar, S. Sen Gupta, *J. Mater. Chem.* **2009**, *19*, 1409.
- [35] X. S. Zhao, G. Q. Lu, A. K. Whittaker, G. J. Millar, H. Y. Zhu, *J. Phys. Chem.* **1997**, *101*, 6525–6531.
- [36] P. Shinde, S. S. Gupta, B. Singh, V. Polshettiwar, B. L. V. Bhagavatula, *J. Mater. Chem. A* **2017**, *5*, 14914–14921.
- [37] W. Kolodziejewski, J. Klinowski, *Chem. Rev.* **2002**, *102*, 613–628.
- [38] M. Kirchhof, K. Gugeler, F. R. Fischer, M. Nowakowski, A. Bauer, S. Alvarez-Barcia, K. Abitaev, M. Schnierle, Y. Qawasmi, W. Frey, A. Baro, D. P. Estes, T. Sottmann, M. R. Ringenberg, B. Plietker, M. Bauer, J. Kästner, S. Laschat, *Organometallics* **2020**, *39*, 3131–3145.
- [39] G. Brogini, G. Poli, E. M. Beccalli, F. Brusa, S. Gazzola, J. Obler, *Adv. Synth. Catal.* **2015**, *357*, 677–682.
- [40] F. Himo, T. Lovell, R. Hilgraf, V. V. Rostovtsev, L. Noodleman, K. B. Sharpless, V. V. Fokin, *J. Am. Chem. Soc.* **2005**, *127*, 210–216.
- [41] a) K. Stawicka, K. Drazkiewicz, M. Ziolek, *Microporous Mesoporous Mater.* **2018**, *258*, 41–54; b) K. Ouhenia-Ouahadi, G. Laurent, E. Barrez, P. Yu R Métivier, A. Déberre, *J. Phys. Chem. C* **2018**, *122*, 6984–6995; c) I. del Hierro, Y. Pérez, P. Cruz, R. Juárez, *Eur. J. Inorg. Chem.* **2017**, *24*, 3030–3039.
- [42] G. E. Negrón-Silva, R. González-Olvera, D. Angeles-Beltrán, N. Maldonado-Carmona, A. Espinoza-Vázquez, M. E. Palomar-Pardavé, M. A. Romero-Romo, R. Santillan, *Molecules* **2013**, *18*, 4613–4627.
- [43] C. Giacovazzo in *Fundamentals of Crystallography*, Third Edition (Ed.: C. Giacovazzo), Oxford University Press, Oxford, **2011**, pp. 161162.
- [44] H. Yang, M. Xu, *Chin. J. Chem.* **2013**, *31*, 119–122.
- [45] J. Nakazawa, B. J. Smith, T. D. P. Stack, *J. Am. Chem. Soc.* **2012**, *134*, 2750–2759.

Manuscript received: February 10, 2021
Revised manuscript received: March 8, 2021
Accepted manuscript online: March 15, 2021
Version of record online: April 9, 2021